Quaternary Science Reviews 188 (2018) 160–166

Contents lists available at ScienceDirect

Quaternary Science Reviews

journal homepage: www.elsevier.com/locate/quascirev

Short Communication

Trans-pacific glacial response to the Antarctic Cold Reversal in the southern mid-latitudes

Esteban A. Sagredo [a, *], Michael R. Kaplan [b], Paola S. Araya [a], Thomas V. Lowell [c], Juan C. Aravena [d], Patricio I. Moreno [e], Meredith A. Kelly [f], Joerg M. Schaefer [b, g]

[a] Instituto de Geografía, Pontificia Universidad Católica de Chile, Santiago, Chile
[b] Lamont-Doherty Earth Observatory of Columbia University, Palisades, NY, 10944, USA
[c] Geology Department, University of Cincinnati, Cincinnati, OH, 45221, USA
[d] Gaia-Antártica, Universidad de Magallanes, Punta Arenas, Chile
[e] Instituto de Ecología y Biodiversidad, Departamento de Ciencias Ecológicas, Universidad de Chile, Santiago, Chile
[f] Department of Earth Sciences, Dartmouth College, Hanover, NH, 03755, USA
[g] Department of Earth and Environmental Sciences of Columbia University, New York, NY, 10027, USA

ARTICLE INFO

Article history:
Received 26 October 2017
Received in revised form
15 January 2018
Accepted 19 January 2018
Available online 31 March 2018

Keywords:
Patagonia
Monte San Lorenzo
Glacier fluctuation
Antarctic Cold Reversal
Late glacial
Southern westerly winds

ABSTRACT

Elucidating the timing and regional extent of abrupt climate events during the last glacial-interglacial transition (~18–11.5 ka) is critical for identifying spatial patterns and mechanisms responsible for large-magnitude climate events. The record of climate change in the Southern Hemisphere during this time period, however, remains scarce and unevenly distributed. We present new geomorphic, chronological, and equilibrium line altitude (ELA) data from a climatically sensitive mountain glacier at Monte San Lorenzo (47°S), Central Patagonia. Twenty-four new cosmogenic ^{10}Be exposure ages from moraines provide a comprehensive glacial record in the mid-latitudes of South America, which constrain the timing, spatial extent and magnitude of glacial fluctuations during the Antarctic Cold Reversal (ACR, ~14.5–12.9 ka). Río Tranquilo glacier advanced and reached a maximum extent at 13.9 ± 0.7 ka. Three additional inboard moraines afford statistically similar ages, indicating repeated glacier expansions or marginal fluctuations over the ACR. Our record represents the northernmost robust evidence of glacial fluctuations during the ACR in southern South America, documenting not only the timing of the ACR maximum, but also the sequence of glacier changes within this climate event. Based on ELA reconstructions, we estimate a cooling of >1.6–1.8 °C at the peak of the ACR. The Río Tranquilo record along with existing glacial reconstructions from New Zealand (43°S) and paleovegetation records from northwestern (41°S) and central-west (45°S) Patagonia, suggest an uniform trans-Pacific glacier-climate response to an ACR trigger across the southern mid-latitudes. We posit that the equatorial migration of the southern westerly winds provides an adequate mechanism to propagate a common ACR signal across the Southern Hemisphere.

© 2018 Elsevier Ltd. All rights reserved.

1. Introduction

The end of the last ice age was interrupted by millennial-scale cold reversals in both polar hemispheres. Antarctic ice cores show a sustained decline in air temperature and cessation of the deglacial CO_2 rise between 14.7 and 12.9 ka (ka: thousand years before present), during the Antarctic Cold Reversal (ACR; Pedro et al., 2011). This was followed by warming at 12.9 ka, coeval with the onset of the Younger Dryas (YD), a climate reversal that plunged winter temperatures to near glacial values in mid-to high-latitudes of the Northern Hemisphere (Denton et al., 2005; Rasmussen et al., 2006) until the onset of the Holocene (11.7 ka).

Research over the last two decades has provided key evidence for validating the ACR signal at mid- and high southern latitudes, however, the mechanisms involved in its generation and propagation remain elusive (e.g., Chiang et al., 2014; Crowley, 1992; Denton et al., 2010; Pedro et al., 2016; Weaver et al., 2003). Furthermore, the spatial extent of the ACR signal across the mid-latitudes of the Southern Hemisphere is insufficiently understood.

* Corresponding author.
E-mail address: esagredo@uc.cl (E.A. Sagredo).

https://doi.org/10.1016/j.quascirev.2018.01.011
0277-3791/© 2018 Elsevier Ltd. All rights reserved.

A recent analysis of a transient paleoclimate simulation and proxy records through the last glacial termination showed statistically significant ACR cooling in records south of 40°S (Pedro et al., 2016). The empirical evidence around the South Pacific basin analyzed in that study, however, is unclear and inconclusive. For example, the assessment revealed (i) strong, statistically significant ACR cooling in a speleothem record from New Zealand's South Island (41°S), (ii) weak or unclear signals in marine and chironomid records from both sides of the Pacific basin (41°-46°S), and (iii) glacier advances in New Zealand and southernmost Patagonia during the ACR (Pedro et al., 2016).

Available glacial records point to an apparent asymmetry in the latitudinal extent of the ACR in the eastern and western sectors of the south Pacific basin. In Patagonia, the northernmost evidence for a glacial advance during the ACR constrained by a robust chronology comes from Lago Argentino, at 50°S (Strelin et al., 2011). Available evidence north of that locale features limited chronologic control, precluding unambiguous assignment of age for climatic events at millenial timescales (Glasser et al., 2012; Turner et al., 2005). In New Zealand available glacial chronologies show ACR glacial advances as far north as 43°S (e.g. Kaplan et al., 2010; Kaplan et al., 2013; Putnam et al., 2010). This difference in latitudinal distribution (i.e., northernmost extent) of glacial advances throughout the ACR might reflect a zonally asymmetric feature in the paleoclimate signal across the southern mid-latitudes, or an artifact of poorly constrained chronologies of glacial change in the Andes north of ~50°S.

We set out to refine the spatial-temporal extent of glacier fluctuations in Patagonia during the ACR interval using a new ^{10}Be chronology of glacial events of Río Tranquilo glacier, a small, simple, and independent mountain glacier located on the northern flank of Monte San Lorenzo (47°35′S; 72°19′W) (Fig. 1).

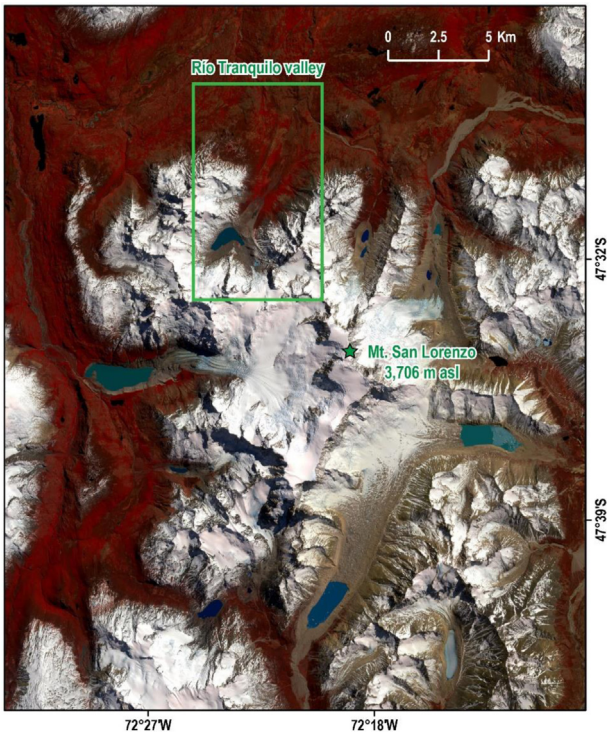

Fig. 1. Río Tranquilo valley, Mt. San Lorenzo. Sentinel 2 image (Infrared, 2016) showing the entire granodioritic San Lorenzo massive and all the glaciers draining from its headwalls. Green box highlights the study area. (For interpretation of the references to colour in this figure legend, the reader is referred to the Web version of this article.)

2. Regional setting

Central Patagonia corresponds to the region located between 44° and 48°S, in southern South America. Moisture-laden southern westerly winds (SWW) deliver more than 4 m a-1 of precipitation on the western flank of the Andes in this region, and sustain the Northern Patagonian Icefield (NPI) (Casassa et al., 1998; Rivera et al., 2007), the second largest icefield outside Antarctica. The moisture content of the SWW diminishes east of the Andes to almost 0.2 m a-1 in extra Andean sectors (Villa-Martínez et al., 2012). Monte San Lorenzo (47°35′S and 72°19′W; 3706 m asl; Chilean name: Monte Cochrane) is a granodiorite massif with an ice-covered area of ca. 140 km^2 (Falaschi et al., 2013), located ~70 km southeast of the NPI. It represents one of the most extensively glaciarized mountains in the region (Caldenius, 1932). Here, we focus on the Río Tranquilo valley, which is located on the northern flank of Monte San Lorenzo. A recent glacier inventory carried out in the area indicates the existence of 16 small glaciers (<5 km^2) in the valley, with a total ice surface of 15 km^2 (Falaschi et al., 2013) (Fig. 1). Sagredo et al. (2017) showed that glaciers at Río Tranquilo valley are more sensitive to changes in temperature than precipitation.

3. Methods

To constrain the age of the former glacial fluctuations, we mapped and determined direct ages of moraines using ^{10}Be surface exposure dating. We collected rock samples (~1 kg) from boulders embedded in or resting in stable positions on moraine ridges. We only selected boulders that did not showed evidence of post-depositional movement, surface erosion, or exhumation (Fig. S1; Supplementary material). Samples were removed from boulder surfaces (upper 5 cm) using a hammer and chisel or the drill and blast method of Kelly (2003). Beryllium was isolated from whole rock samples at the Lamont-Doherty Earth Observatory Cosmogenic Dating Laboratory (Columbia University), and at the Cosmogenic Nuclide Laboratory (Dartmouth College), following Schaefer et al. (2009). ^{10}Be/Be isotope ratios were measured at the Center for Accelerator Mass Spectrometry at Lawrence Livermore National Laboratory (CAMS LLNL). Geographical and analytical data of the samples are provided in Table 1.

Be ages were calculated based on the methods incorporated in the CRONUS-Earth online exposure age calculators. In more detail, we used version 2.2, with version 2.2.1 of the constants file (Balco et al., 2008), and with a high-resolution version of the geomagnetic framework (Lifton et al., 2008), to be consistent with calculations in Kaplan et al. (2011). We calculated all ages using the regional Patagonian production rate and assuming zero erosion; if a global rate (e.g., Borchers et al., 2016) is used with ^{10}Be concentrations at the production rate sites in Patagonia, ages are generally too young compared with the limiting ^{14}C data (Kaplan et al., 2011). Ages presented here are based on the time dependent version of Stone/Lal (Lal, 1991; Stone, 2000) scaling protocol scheme (Lm). For comparison, the use of other scaling schemes (e.g. LSD) and systematic differences (i.e., from those explained in Kaplan et al., 2011), including those incorporated into recent versions of online calculators, afford ages that are lower by about 2–3%, from those presented here. Hence, choice of scaling models and version of the online calculator do not affect our conclusions. We report individual ^{10}Be ages with 1σ analytical uncertainty. Mean moraine ages include the propagation of the analytical uncertainty and the uncertainty of the local production rate (3%).

We estimated modern and former ELAs using the Accumulation Area Ratio (AAR) method (Porter, 2001) (for details and discussion on the application of the AAR method, see Supplementary material: ELA reconstruction). In our study, we apply the average AAR ratio

Table 1
Geographical and analytical data for samples from Río Tranquilo valley. AMS standard used for normalization is 07KNSTD with a reported $^{10}Be/^{9}Be$ value of 2.85×10^{-12} (Nishiizumi et al., 2007; ^{10}Be half life = 1.36 Myr). 1σ analytical or internal AMS uncertainties are shown. Density = 2.65 g/cm^3. (*) = Samples prepared at the Lamont-Doherty Earth Observatory Cosmogenic Dating Laboratory (Columbia University). (**) = Samples prepared at the Cosmogenic Nuclide Laboratory (Dartmouth College). Carrier concentrations as follow: ([a])1.014 ppt, ([b]) 1.035 ppt, ([c]) 1.037 ppt and ([d]) 1.314 ppt. Four blanks were processed with the samples and their $^{10}Be/^{9}Be$ ratios ranged from 1.15×10^{-16} to 8.67×10^{-16}. RmE = Remnant ridge east. RmW = Remnant ridge west.

Moraine	Sample	CAMS number	Lat (°)	Long (°)	Elevation (m. asl)	Thickness (cm)	Shielding	Quartz wt (g)	^{9}Be Carrier (mg)	$^{10}Be/^{9}Be$ (10^{-14})	^{10}Be (10^4 atoms g^{-1})
RT1	PC13-01-01 *	BE36353	−47.4936	−72.4936	913	1.9	0.9854	7.0411	0.1843 [a]	6.69 ± 0.16	11.69 ± 0.27
	PC13-01-02 *	BE36354	−47.4894	−72.4894	884	1.7	0.9900	7.0731	0.1843 [a]	6.83 ± 0.16	11.88 ± 0.28
	PC13-01-05 *	BE37443	−47.4873	−72.3569	881	1.5	0.9952	4.5813	0.1873 [b]	4.42 ± 0.22	12.12 ± 0.61
	PC13-01-06 *	BE38765	−47.4837	−72.3559	811	1.0	0.9981	10.0354	0.1873 [c]	9.23 ± 0.20	11.62 ± 025
	PC13-01-29 *	BE37444	−47.4809	−72.3778	835	2.3	0.9947	5.8103	0.1864 [b]	4.99 ± 0.14	10.75 ± 0.31
	PC14-01-18 *	BE38775	−47.4816	−72.3780	873	1.9	0.9982	6.4810	0.1870 [c]	5.88 ± 0.12	11.43 ± 0.24
	PC14-01-22 *	BE38772	−47.4929	−72.3834	932	1.7	0.9954	8.1965	0.1864 [c]	8.31 ± 0.17	12.74 ± 0.26
	PC14-01-23 *	BE38773	−47.4933	−72.3836	927	3.2	0.9957	10.0129	0.1863 [c]	10.45 ± 0.26	13.12 ± 0.33
RT2	PC10-01-08 **	BE32426	−47.4754	−72.3728	788	1.7	0.9983	6.0705	0.1634 [d]	4.68 ± 0.14	11.07 ± 0.33
RT2r	PC10-01-10 *	BE37440	−47.4760	−72.3735	789	2.0	0.9957	7.0279	0.1865 [b]	5.64 ± 0.17	10.06 ± 0.31
RT3	PC10-01-24 *	BE37442	−47.4803	−72.3740	762	2.0	0.9946	7.1004	0.1853 [b]	5.94 ± 0.14	10.41 ± 0.25
	PC10-01-14 *	BE37441	−47.4857	−72.3773	783	6.0	0.9765	7.0159	0.1858 [b]	7.29 ± 0.16	12.98 ± 0.28
	PC10-01-23 *	BE38771	−47.4807	−72.3711	730	1.5	0.9932	10.0421	0.1864 [c]	8.00 ± 0.17	10.01 ± 0.21
RT4	PC10-01-11 **	BE32427	−47.4887	−72.3770	781	2.8	0.9830	5.9895	0.1649 [d]	4.54 ± 0.14	10.98 ± 0.34
	PC10-01-12 **	BE32428	−47.4890	−72.3778	785	0.7	0.9916	5.9850	0.1622 [d]	4.58 ± 0.14	10.91 ± 0.33
	PC10-01-13 **	BE32429	−47.4992	−72.3782	792	4.3	0.9789	6.0361	0.1616 [d]	6.93 ± 0.17	16.28 ± 0.40
	PC10-01-16 **	BE32430	−47.4836	−72.3719	739	1.1	0.9881	6.0659	0.1616 [d]	4.51 ± 0.15	10.55 ± 0.36
RT5	PC10-01-20 *	BE38769	−47.4784	−72.3702	732	2.5	0.9966	4.9814	0.1868 [c]	3.96 ± 0.10	9.98 ± 0.26
	PC10-01-22 *	BE38770	−47.4840	−72.3705	730	3.5	0.9950	10.0149	0.1881 [c]	7.93 ± 0.15	10.05 ± 0.19
	PC13-01-27 *	BE36358	−47.4952	−72.3785	754	3.3	0.9780	4.3813	0.1848 [a]	3.33 ± 0.11	9.35 ± 0.31
	PC13-01-28 *	BE36359	−47.4960	−72.3800	765	1.3	0.9776	7.0950	0.1847 [a]	5.11 ± 0.17	8.87 ± 0.30
RT6	PC10-01-17 **	BE32431	−47.5278	−72.3912	1291	2.0	0.9841	27.5379	0.1623 [d]	12.62 ± 0.24	6.53 ± 0.13
	PC10-01-18 **	BE32432	−47.5273	−72.3912	1281	1.3	0.9770	35.7078	0.1620 [d]	16.74 ± 0.24	6.67 ± 0.17
	PC10-01-19 **	BE32433	−47.5270	−72.3912	1277	2.7	0.9804	37.7215	0.1616 [d]	16.41 ± 0.31	6.17 ± 0.12
RmE	PC13-01-03 *	BE36355	−47.4881	−72.3566	878	2.3	0.9941	7.0418	0.1848 [a]	7.52 ± 0.16	13.17 ± 0.28
	PC13-01-04 *	BE36356	−47.4881	−72.3566	879	2.2	0.9928	7.0492	0.1850 [a]	8.12 ± 0.17	14.22 ± 0.30
RmW	PC14-01-21 *	BE38776	−47.4891	−72.3819	917	1.4	0.9931	2.5388	0.1668 [c]	3.91 ± 0.16	17.26 ± 0.71

0.67 (2:3) (Chinn and Whitehouse, 1980). Since it is very likely that the modern glacier is in a transient equilibrium, we argue that the AAR value used for the present-day glacier is conservative, and therefore the modern ELA and the ELA difference estimates represent minimum values.

4. Results

A comprehensive geomorphic survey allowed identification of at least six groups of distinct well-preserved moraines within the Río Tranquilo (RT) valley. These are named informally RT1 to RT6, from the outermost to the innermost moraine groups.

The outermost moraines (RT1) comprise two prominent and well-delineated lateral ridges (one on each side of the valley) that reach up to 200 m above both sides of the valley floor. For the majority of their extent these moraines exhibit a single crest; some areas, however, exhibit remnants of secondary ridges just outside the main crest. Eight samples collected from these features yielded ages ranging from 14.9 ± 0.4 to 13.1 ± 0.4 ka, with a mean of 13.9 ± 0.7 ka (Fig. 2 and Table 2). Although these ages exhibit significant spread, there is no statistical basis for excluding any ages; furthermore, all ages fall within 2σ of the average. The main RT1 ridge bifurcates near its distal end forming another moraine (RT2) that curves toward the Río Tranquilo river, partially enclosing the valley ~8.5 km from the present-day ice margin. Two samples from the main ridge of RT2 yielded ages of 13.9 ± 0.4 and 12.7 ± 0.4 ka. Immediately inboard, we identified a sequence of subdued recessional moraine ridges (RT2r). A ^{10}Be date from a single boulder atop one of these moraines yielded an age of 13.5 ± 0.3 ka. RT3 and RT4 are the next two groups of moraines farther upstream. They include multiple well-defined ridges, originating from the flank of the RT1 moraines, and enclose the valley 7.6 and 7.1 km from the present-day ice margin, respectively. An outwash plain originated from RT4 separates both systems and partially buried the RT3 moraines. One sample from the RT3 moraines yielded an age of 17.2 ± 0.4 ka (sample PC10-01-14) which we excluded because it is anomalously old and out of morphostratigraphic sequence. Five boulders from the RT4 moraines yielded ages ranging from 14.2 ± 0.4 to 13.3 ± 0.3 ka, with a mean of 13.7 ± 0.5 ka (sample PC10-01-13 was excluded based on a Grubbs's test for outliers; Grubbs, 1969). Approximately 600 m farther upstream and more than 2 km from the R1 moraine, we identified another set of moraines (RT5), which describes an elongated arc on the west side of the river (on the eastern side this feature has been intensively eroded by fluvial processes and only few remnants are preserved). Unlike the older moraines, RT5 is restricted to the valley bottom at lower elevations, implying a lower ice surface; two boulder dates from these moraines yielded ages of 12.5 ± 0.4 and 11.6 ± 0.4 ka. Further upstream, we find the RT6 moraines, which comprise between five and seven well defined ridges that enclose the valley ~3.5 km from the present ice margin. Sagredo et al. (2017) reported three ^{10}Be ages from a single ridge in the middle of this moraine sequence with ages ranging from 5.4 ± 0.1 to 5.8 ± 0.1 ka (mean = 5.6 ± 0.3 ka). Finally, we obtained three ages on small remnants of an old moraine(s), immediately outside the lateral crests of RT1. There, boulders yielded ages of 15.5 ± 0.3, 16.7 ± 0.4 ka (right lateral) and 19.5 ± 0.8 ka (left lateral), defining the maximum age-limit of the entire late glacial moraine sequence.

We estimated the ELA for the present-day and former (RT2, RT3 and RT4 positions) Río Tranquilo glacier using the Accumulation Area Ratio method (AAR; e.g., Porter, 2001) (Fig. S4; Supplementary material); the absence of the frontal RT1 moraine precludes precise reconstruction of the ELA for the ACR maximum position. Our results show that when the ice margin reached the RT2 moraine, the ELA was 260 ± 20 m below modern values. Because of the proximity of RT3 and RT4 moraines, our calculations show that during both

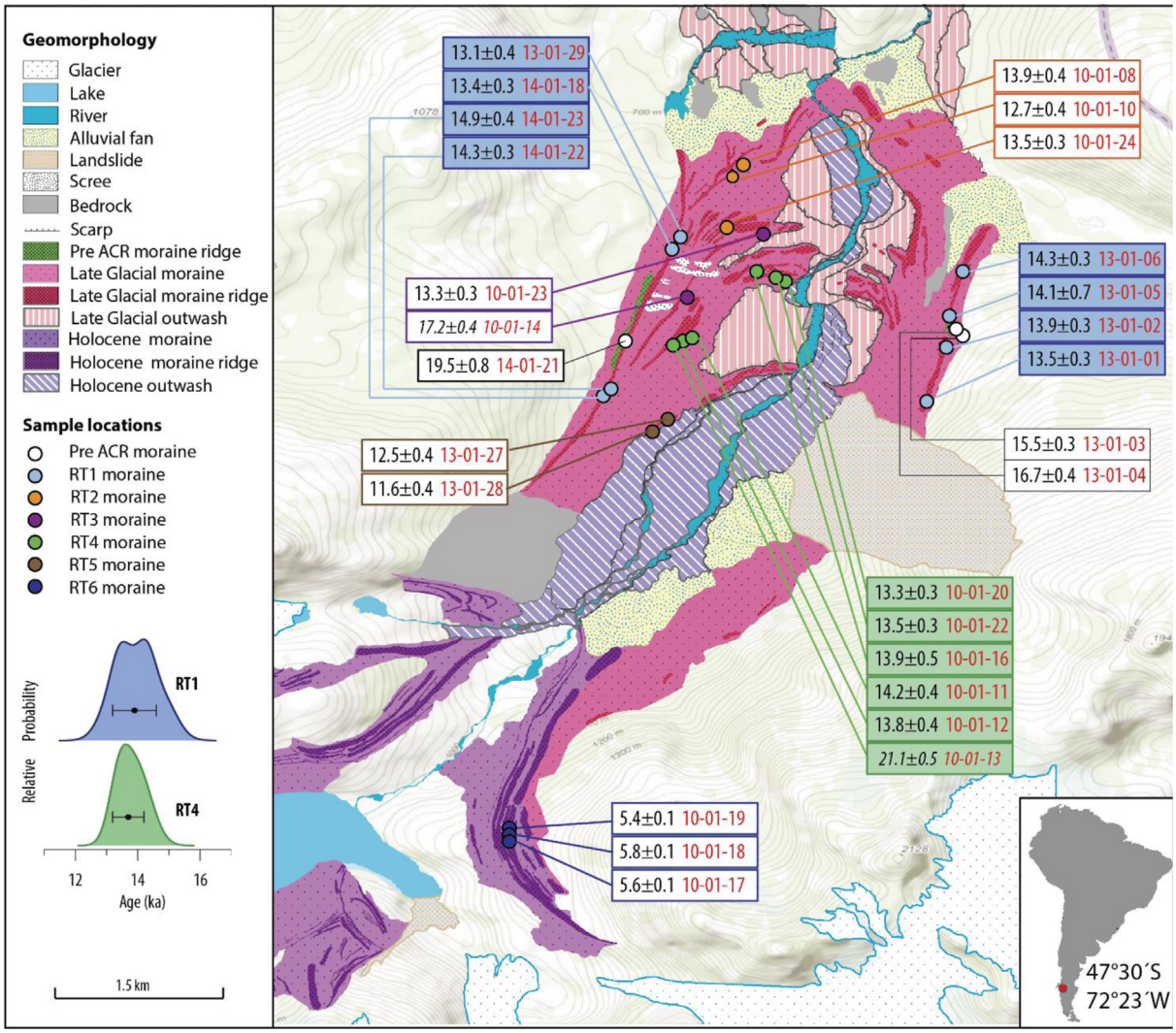

Fig. 2. Glacial geomorphologic map of the Río Tranquilo valley. Individual ^{10}Be ages (in ka) are provided with 1σ analytical uncertainty (Table 2). We omitted the prefix "PC" in the sample code. Outliers are shown in italics. Dates highlighted in blue and green boxes are from the outermost and innermost ACR moraines, RT1 and RT4, respectively. In legend, RT1 and RT4 mean moraine ages (±1σ including a 3% production-rate uncertainty propagated) are shown, along with the corresponding summed probability distribution plot of the age population. (For interpretation of the references to colour in this figure legend, the reader is referred to the Web version of this article.)

events the ELA depression was statistically indistinguishable, with estimates of 210 ± 20 m (RT3) and 200 ± 20 m (RT4). Considering that by the time of deposition of RT2 the glacier was smaller than during the RT1, the above ELA depression estimates are considered minimum values for the latter in central Patagonia. If we assume that the ELA depression during the LGM in the central Patagonian region was ~900 m (Hubbard et al., 2005), our estimate for ELA lowering of Río Tranquilo glacier during the ACR represents almost one third of this value. Assuming an adiabatic lapse rate of 6.5 °C/1000 m and no changes in precipitation, the estimated ELA depressions translate in temperatures of anomalies relative to the present of 1.6–1.8 °C (for RT2), 1.2–1.5 °C (for RT3) and 1.2–1.4 °C (for RT4).

5. Discussion

The four most prominent moraine groups (RT1-RT4) in the Río Tranquilo valley were deposited during the ACR, with individual boulder ages spanning from 14.9 ± 0.4 to 12.7 ± 0.4 ka. Morphostratigraphic and chronological evidence suggests that Río Tranquilo glacier reached its maximum by 13.9 ± 0.7 ka (RT1). The ice then remained in an extended position slightly inboard of the maximum, depositing three moraines in relatively close succession (RT2-RT4). The age of RT4 moraine is statistically indistinguishable from RT1 (13.7 ± 0.5 ka); however, morphostratigraphically, RT4 represent the end of the ACR moraine sequence in this area. Río Tranquilo glacier then underwent recession and thinning, punctuated by a stabilization or readvance (RT5). The next documented advance, after a long period of glacier retreat, took place during the mid-Holocene (RT6 = 5.6 ± 0.3 ka).

Individual moraines dated within the ACR interval have been recorded farther south in Patagonia (i.e., 50° - 55°S) (e.g., Ackert et al., 2008; García et al., 2012; Glasser et al., 2011; Kaplan et al., 2008; Menounos et al., 2013; Moreno et al., 2009; Strelin et al., 2011); most of these moraines were deposited by large outlet glaciers of the former Patagonian ice sheet (Fig. 3). Our comprehensive chronology from a small sensitive mountain glacier not only shows the timing of the ACR maximum, but also the sequence of glacier changes within this climate event. Thus, our results constitute the northernmost detailed expression of glacial activity during the ACR in the mid-latitudes of South America, and reveal that glaciers responded to the ACR cooling to at least as far north as 47°S.

Table 2
^{10}Be ages (ka) from Río Tranquilo valley, based on the time dependent version of Stone/Lal (Lal, 1991; Stone, 2000) scaling protocol scheme. Individual age uncertainties include only the analytical error (i.e., machine measurement uncertainty), otherwise known as internal error (Balco et al., 2008). RT2r = RT2 recessional. (*) in Sagredo et al. (2017). RmE = Remnant ridge east. RmW = Remnant ridge west.

Moraine	Sample ID	Age	±1σ
	PC13-01-01	13.5	0.3
	PC13-01-02	13.9	0.3
	PC13-01-05	14.1	0.7
RT1	PC13-01-06	14.3	0.3
	PC13-01-29	13.1	0.4
	PC14-01-18	13.4	0.3
	PC14-01-22	14.3	0.3
	PC14-01-23	14.9	0.4
RT2	PC10-01-08	13.9	0.4
	PC10-01-10	12.7	0.4
RT2r	PC10-01-24	13.5	0.3
RT3	*PC10-01-14*	*17.2*	*0.4*
	PC10-01-23	13.3	0.3
	PC10-01-11	14.2	0.4
	PC10-01-12	13.8	0.4
RT4	*PC10-01-13*	*21.1*	*0.5*
	PC10-01-16	13.9	0.5
	PC10-01-20	13.3	0.3
	PC10-01-22	13.5	0.3
RT5	PC13-01-27	12.5	0.4
	PC13-01-28	11.6	0.4
	PC10-01-17	5.6	0.1
RT6 (*)	PC10-01-18	5.8	0.1
	PC10-01-19	5.4	0.1
RmE	PC13-01-03	15.5	0.3
	PC13-01-04	16.7	0.4
RmW	PC14-01-21	19.5	0.8

Previous studies have shown minor stabilizations/readvances of Patagonian glaciers (50°-51°S) during the YD chron, inboard the ACR glacial limits (Moreno et al., 2009; Sagredo et al., 2011; Strelin et al., 2011). We suggest that the deposition of RT5 occurred during YD time but acknowledge that additional dates are needed to substantiate this finding on firmer geochronologic ground.

Our chronology from Río Tranquilo glacier also matches similar events reported much further north (43°S), on the opposite side of the South Pacific basin, in the Southern Alps of New Zealand (Fig. 3). Those studies document glacial advances ending by ~13 ka (Kaplan et al., 2010, 2013; Putnam et al., 2010; Turney et al., 2007), followed by net recession punctuated by still-stands or minor readvances during the YD chron (Kaplan et al., 2010). Our results offer new evidence of the millennial-scale structure of the last glacial to interglacial transition throughout the southern mid-latitudes.

The ACR signal has also been recorded in paleovegetation records from southern South America, but the spatial distribution of its footprint is still unclear. Pollen records from northwestern Patagonia (41°-43°S) show increases in cold-resistant hygrophilous conifers, interpreted as a shift toward cold/wet conditions during the ACR, followed by intense fire activity driven by enhanced precipitation variability during the YD (Moreno, 2004; Moreno and León, 2003; Moreno and Videla, 2016; Pesce and Moreno, 2014). Evidence for these events in central-west Patagonia still remains elusive (Bennett et al., 2000; Haberle and Bennett, 2004; Villa-Martínez et al., 2012). Recently, Henríquez et al. (2017) reported a pollen record from Lago Edita (45°S, 45 km north of Mt. San Lorenzo) that features the same palynological signal found in northwestern Patagonian sites (i.e. a rise in *Podocarpus nubigena* between 14.5 and 11 ka) with a cold-wet early portion (14.5–13 ka), followed by a gradual rise in arboreal pollen (chiefly *Nothofagus*) and large-magnitude fires between 13 and 11 ka. Henríquez et al. (2017) interpreted the latter as a warm pulse under predominantly wet

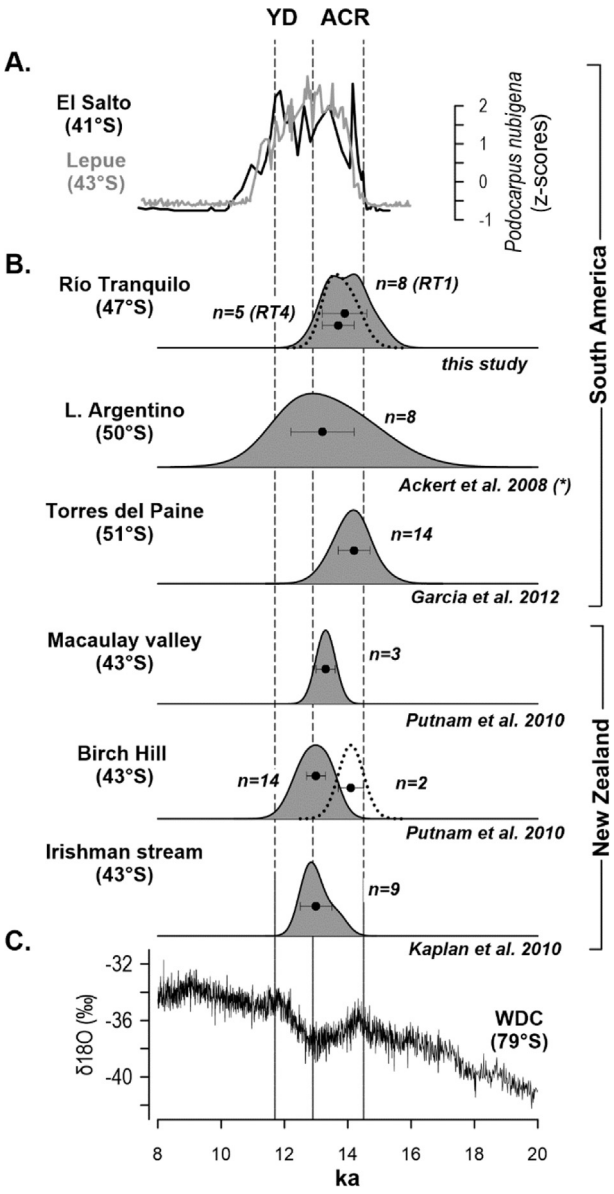

Fig. 3. Late glacial climate as shown in glacier and climate records across the mid- and high latitudes of the Southern Hemisphere. **A.** Variations in hygrophilous cold-resistant conifer *Podocarpus nubigena* in pollen records from Lago El Salto (Moreno and Videla, 2016) and Lago Lepué (Pesce and Moreno, 2014), northwestern Patagonia. Higher (lower) values represent cold and wet (warm and dry) conditions. Both records show cold conditions during the ACR and YD chrons with high/lower precipitation regime during the former/latter (Moreno and Videla, 2016). **B.** ^{10}Be chronologies of advances in southern mid-latitude glaciers during the ACR. We show the summed probability distribution curves of the age population of the outermost moraines during the time period. In the case of Río Tranquilo, we also included the summed probability plot of the innermost ACR moraine; for Birch Hill we included the summed probability plot of a small moraine remnant immediately outboard of the main moraine complex. (*) Ages were recalibrated in Kaplan et al. (2011). **C.** δ^{18}O from central West Antarctica ice core (WAIS Divide Project Members, 2015). Dashed vertical lines define the ACR and YD chrons.

but highly variable precipitation regime, suggesting that cold-wet climate during the ACR gave way to milder temperate conditions and highly variable southern westerly winds (SWW) during YD time in central-west Patagonia. Our data from Río Tranquilo valley are fully consistent with these palynological studies, namely: maximum glacier extent during cold-wet ACR climate, followed by thinning, recession, and the potential stabilization and lingering of

ice during YD time under milder climate with enhanced SWW variability.

Combined with previous data, our findings from a small, temperature-sensitive glacier suggest that the ACR cooling signal extends throughout the entire Patagonian region. In conjunction with glacial chronologies from New Zealand (43°- 44°S) and Antarctic ice core data (e.g., WAIS Divide Ice: 79°S) our results provide firm evidence for a common atmospheric cooling during the ACR along a zonally symmetric trans-Pacific band between 79° and 41°S (Fig. 3).

To explain the widespread trans-Pacific distribution of glacier advances during the ACR, we propose an equatorial migration of the SWW and associated mid-high latitude climates (Moreno et al., 2012; Pesce and Moreno, 2014; Putnam et al., 2010). Northward-shifted SWW generate conditions that would favor positive mass balance (reduced summer temperature and enhanced annual precipitation) throughout western Patagonia and New Zealand (Garreaud et al., 2013), eliciting widespread glacial advances throughout mid-latitudes of the Southern Hemisphere.

This scenario, of an equatorward migration of the SWW, is also linked to a decline in upwelling in the Atlantic sector of the Southern Ocean (Anderson et al., 2009) and a cessation in the deglacial rise of atmospheric CO_2 (Marcott et al., 2014; Monnin et al., 2001; Pedro et al., 2012) during the ACR. In addition, Toggweiler et al. (2006) suggested that the northward migration of the SWW also leads to the northward shift of the Subtropical Front; this process, combined with the reduction of upwelling in the Southern Ocean, favors the expansion of sea ice around Antarctica (Putnam et al., 2010). A recent deuterium excess record from WAIS supports the idea that SWW shifts to the north in the Pacific during Antarctica cold stages (Markle et al., 2017). Thus, although the initial (global) trigger is still elusive, a migration of the SWW and associated climate belts provides an adequate mechanism to explain the propagation of a unified ACR signal in the Southern Hemisphere.

Acknowledgements

This work was funded by Iniciativa Científica Milenio NC120066, FONDECYT 11121280, 1160488, and 1151469, CONICYT USA 2013-0035 NSF-BCS 1263474 and a Fulbright Visiting Scholar Grant (Kaplan). We thank R. Schwartz, J. Hanley, J. Frisch and J. Howley for laboratory assistance. Our appreciation goes to CEQUA, J. Araos, I. González, F. González, B. Luckman, J. Koch, L. Soto and L. Gómez, for providing field assistance. This is LDEO contribution #8180.

Appendix A. Supplementary data

Supplementary data related to this article can be found at https://doi.org/10.1016/j.quascirev.2018.01.011.

References

Ackert, R.P., Becker, R.A., Singer, B.S., Kurz, M.D., Caffee, M.W., Mickelson, D.M., 2008. Patagonian glacier response during the late glacial–Holocene transition. Science 321 (5887), 392–395.
Anderson, R.F., Ali, S., Bradtmiller, L.I., Nielsen, S.H.H., Fleisher, M.Q., Anderson, B.E., Burckle, L.H., 2009. Wind-driven upwelling in the Southern Ocean and the deglacial rise in atmospheric CO2. Science 323, 1443–1448.
Balco, G., Stone, J.O., Lifton, N.A., Dunai, T.J., 2008. A complete and easily accessible means of calculating surface exposure ages or erosion rates from 10Be and 26Al measurements. Quat. Geochronol. 3, 174–195.
Bennett, K.D., Haberle, S.G., Lumley, S.H., 2000. The last glacial-Holocene transition in southern Chile. Science 290 (5490), 325–328.
Borchers, B., Marrero, S., Balco, G., Caffee, M., Goehring, B., Lifton, N., Nishiizumi, K., Phillips, F., Schaefer, J., Stone, J., 2016. Geological calibration of spallation production rates in the CRONUS-Earth project. Quat. Geochronol. 31, 188–198.
Caldenius, C., 1932. Las Glaciaciones Cuaternarias en la Patagonia y Tierra del Fuego. Geogr. Ann. 14, 1–164.
Casassa, G., Espizua, L.E., Francou, B., Ribstein, P., Ames, A., Aleans, J., 1998. Glaciers in south America. In: Haeberli, W., Hoelzle, M., Suter, S. (Eds.), Into the Second Century of Worldwide Glacier Monitoring - Prospects and Strategies. UNESCO, Paris.
Chiang, J.C., Lee, S.-Y., Putnam, A.E., Wang, X., 2014. South Pacific Split Jet, ITCZ shifts, and atmospheric North–South linkages during abrupt climate changes of the last glacial period. Earth Planet Sci. Lett. 406, 233–246.
Chinn, T., Whitehouse, I., 1980. Glacier snow line variations in the Southern Alps, New Zealand. IAHS-AISH Publ. 126, 219–228.
Crowley, T.J., 1992. North Atlantic deep water cools the southern hemisphere. Paleoceanography 7 (4), 489–497.
Denton, G.H., Alley, R.B., Comer, G.C., Broecker, W.S., 2005. The role of seasonality in abrupt climate change. Quat. Sci. Rev. 24, 1159–1182.
Denton, G.H., Anderson, R.F., Toggweiler, J.R., Edwards, R.L., Schaefer, J.M., Putnam, A.E., 2010. Tha last glacial termination. Science 328, 1652–1656.
Falaschi, D., Bravo, C., Masiokas, M., Villalba, R., Rivera, A., 2013. First glacier inventory and recent changes in glacier area in the Monte San Lorenzo region (47°S), southern Patagonian Andes, South America. Arctic Antarct. Alpine Res. 45 (1), 19–28.
García, J.L., Kaplan, M.R., Hall, B.L., Schaefer, J.M., Vega, R.M., Schwartz, R., Finkel, R., 2012. Glacier expansion in southern Patagonia throughout the Antarctic cold reversal. Geology 40 (9), 859–862.
Garreaud, R., Lopez, P., Minvielle, M., Rojas, M., 2013. Large-scale control on the Patagonian climate. J. Clim. 26 (1), 215–230.
Glasser, N.F., Harrison, S., Schnabel, C., Fabel, D., Jansson, K.N., 2012. Younger Dryas and early Holocene age glacier advances in Patagonia. Quat. Sci. Rev. 58, 7–17.
Glasser, N.F., Jansson, K.N., Goodfellow, B.W., de Angelis, H., Rodnight, H., Rood, D.H., 2011. Cosmogenic nuclide exposure ages for moraines in the Lago san martin valley, Argentina. Quat. Res. 75 (3), 636–646.
Grubbs, F.E., 1969. Procedures for detecting outlying observations in samples. Technometrics 11 (1), 1–21.
Haberle, S., Bennett, K., 2004. Postglacial formation and dynamics of north patagonian rainforest in the chonos archipelago, southern Chile. Quat. Sci. Rev. 23 (23), 2433–2452.
Henríquez, W.I., Villa-Martínez, R., Vilanova, I., Pol-Holz, R.D., Moreno, P.I., 2017. The Last Glacial Termination on the Eastern Flank of the Central Patagonian Andes (47°S): Climate of the Past Discussions.
Hubbard, A., Hein, A.S., Kaplan, M.R., Hulton, N.R., Glasser, N., 2005. A modelling reconstruction of the last glacial maximum ice sheet and its deglaciation in the vicinity of the Northern Patagonian Icefield, South America: geografiska Annaler. Series A, Physical Geography 87 (2), 375–391.
Kaplan, M.R., Moreno, P.I., Rojas, M., 2008. Glacial dynamics in southernmost South America during Marine Isotope Stage 5e to the Younger Dryas chron: a brief review with a focus on cosmogenic nuclide measurements. J. Quat. Sci. 23 (6–7), 649–658.
Kaplan, M.R., Schaefer, J.M., Denton, G.H., Barrell, D.J.A., Chinn, T.J.H., Putnam, A.E., Andersen, B.G., Finkel, R.C., Schwartz, R., Doughty, A.M., 2010. glacier retreat in New Zealand during the younger Dryas stadial. Nature 467 (7312), 194–197.
Kaplan, M.R., Schaefer, J.M., Denton, G.H., Doughty, A.M., Barrell, D.J., Chinn, T.J., Putnam, A.E., Andersen, B.G., Mackintosh, A., Finkel, R.C., 2013. The anatomy of long-term warming since 15 ka in New Zealand based on net glacier snowline rise. Geology 41 (8), 887–890.
Kaplan, M.R., Strelin, J.A., Schaefer, J.M., Denton, G.H., Finkel, R.C., Schwartz, R., Putnam, A.E., Vandergoes, M.J., Goehring, B.M., Travis, S.G., 2011. In-situ cosmogenic 10Be production rate at Lago Argentino, Patagonia: implications for late-glacial climate chronology. Earth Planet Sci. Lett. 309, 21–32.
Kelly, M.A., 2003. The Late Wurmian Age in the Western Swiss Alps - Last Glacial Maximum (LGM) Ice-surface Reconstruction and 10Be Dating of Late-glacial Features. Ph.D. dissertation. University of Bern, 105 pp.
Lal, D., 1991. Cosmic ray labeling of erosion surfaces: in-situ nuclide production rates and erosion models. Earth Planet Sci. Lett. 104, 424–439.
Lifton, N., Smart, D., Shea, M., 2008. Scaling time-integrated in situ cosmogenic nuclide production rates using a continuous geomagnetic model. Earth Planet Sci. Lett. 268, 190–201.
Marcott, S.A., Bauska, T.K., Buizert, C., Steig, E.J., Rosen, J.L., Cuffey, K.M., Fudge, T., Severinghaus, J.P., Ahn, J., Kalk, M.L., 2014. Centennial-scale changes in the global carbon cycle during the last deglaciation. Nature 514 (7524), 616.
Markle, B.R., Steig, E.J., Buizert, C., Schoenemann, S.W., Bitz, C.M., Fudge, T., Pedro, J.B., Ding, Q., Jones, T.R., White, J.W., 2017. Global atmospheric teleconnections during Dansgaard-Oeschger events. Nat. Geosci. 10 (1), 36–40.
Menounos, B., Clague, J.J., Osborn, G., Davis, P.T., Ponce, F., Goehring, B., Maurer, M., Rabassa, J., Coronato, A., Marr, R., 2013. Latest Pleistocene and Holocene glacier fluctuations in southernmost Tierra del Fuego, Argentina. Quat. Sci. Rev. 77, 70–79.
Monnin, E., Indermuhle, A., Dallenbach, A., Fluckiger, J., Stauffer, B., Stocker, T., Raynaud, D., Barnola, J.M., 2001. Atmospheric CO2 concentrations over the last glacial termination. Science 291, 112–114.
Moreno, P., Villa-Martínez, R., Cárdenas, M., Sagredo, E., 2012. Deglacial changes of the southern margin of the southern westerly winds revealed by terrestrial records from SW Patagonia (52° S). Quat. Sci. Rev. 41, 1–21.
Moreno, P.I., 2004. Millennial-scale climate variability in northwest Patagonia over the last 15 000 yr. J. Quat. Sci. 19 (1), 35–47.
Moreno, P.I., Kaplan, M.R., Francois, J.P., Villa-Martínez, R.P., Moy, C.M., Stern, C.R., Kubik, P.W., 2009. Renewed glacial activity during the Antarctic cold reversal

and persistence of cold conditions until 11.5 ka in southwestern Patagonia. Geology 37 (4), 375–378.
Moreno, P.I., León, A., 2003. Abrupt vegetation changes during the last glacial to Holocene transition in mid-latitude South America. J. Quat. Sci. 18, 787–800.
Moreno, P.I., Videla, J., 2016. Centennial and millennial-scale hydroclimate changes in Northwestern Patagonia since 16,000 yr BP. Quat. Sci. Rev. 149, 326–337.
Nishiizumi, K., Imamura, M., Caaffee, M.W., Southon, J., Finkel, R.C., McAnich, J., 2007. Absolute calibration of 10Be AMS standards. Nucl. Instrum. Methods Phys. Res. Sect. B 258, 403–413.
Pedro, J., Van Ommen, T., Rasmussen, S., Morgan, V., Chappellaz, J., Moy, A., Masson-Delmotte, V., Delmotte, M., 2011. The last deglaciation: timing the bipolar seesaw. Clim. Past 7, 671–683.
Pedro, J.B., Bostock, H.C., Bitz, C.M., He, F., Vandergoes, M.J., Steig, E.J., Chase, B.M., Krause, C.E., Rasmussen, S.O., Markle, B.R., 2016. The spatial extent and dynamics of the Antarctic Cold Reversal. Nat. Geosci. 9, 51–56.
Pedro, J.B., Rasmussen, S.O., van Ommen, T.D., 2012. Tightened constraints on the time-lag between Antarctic temperature and CO 2 during the last deglaciation. Clim. Past 8 (4), 1213–1221.
Pesce, O., Moreno, P., 2014. Vegetation, fire and climate change in central-east Isla Grande de Chiloé (43 S) since the Last Glacial Maximum, northwestern Patagonia. Quat. Sci. Rev. 90, 143–157.
Porter, S.C., 2001. Snowline depression in the tropics during the last glaciation. Quat. Sci. Rev. 20, 1067–1091.
Putnam, A.E., Denton, G.H., Schaefer, J.M., Barrell, D.J.A., Andersen, B.G., Finkel, R.C., Schwartz, R., Doughty, A.M., Kaplan, M.R., Schlüchter, C., 2010. glacier advance in southern middle-latitudes during the antarctic cold reversal. Nat. Geosci. 3 (10), 700–704.
Rasmussen, S.O., Andersen, K.K., Svensson, A., Steffensen, J.P., Vinther, B.M., Clausen, H.B., Siggaard-Andersen, M.L., Johnsen, S.J., Larsen, L.B., Dahl-Jensen, D., 2006. A new Greenland ice core chronology for the last glacial termination (1984–2012). J. Geophys. Res.: Atmosphere 111 (D6).
Rivera, A., Benham, T., Casassa, G., Bamber, J., Dowdeswell, J., 2007. Ice elevation and areal changes of glaciers from the Northern Patagonia icefield, Chile. Global Planet. Change 58, 126–137.
Sagredo, E.A., Lowell, T.V., Kelly, M.A., Rupper, S., Aravena, J.C., Ward, D.J., Malone, A.G.O., 2017. Equilibrium line altitudes along the Andes during the Last millenium: paleoclimatic implications. Holocene 27 (7), 1019–1033.
Sagredo, E.A., Moreno, P.I., Villa-Martínez, R.P., Kaplan, M.R., Kubik, P.W., Stern, C.R., 2011. Fluctuations of the última esperanza ice lobe (52°S), chilean Patagonia, during the last glacial maximum and termination 1. Geomorphology 125 (1), 92–108.
Schaefer, J.M., Denton, G.H., Kaplan, M.R., Putnam, A., Finkel, R.C., Barrell, D.J., Andersen, B.G., Schwartz, R., Mackintosh, A., Chinn, T., Schluchter, C., 2009. High-frequency Holocene glacier fluctuations in New Zealand differ from the northern signature. Science 324, 622–625.
Stone, J.O., 2000. Air pressure and cosmogenic isotope production. J. Geophys. Res. 105, 23753–23759.
Strelin, J.A., Denton, G.H., Vandergoes, M.J., Ninnemann, U.S., Putnam, A.E., 2011. Radiocarbon chronology of the late-glacial puerto banderas moraines, southern patagonian icefields, Argentina. Quat. Sci. Rev. 30, 2551–2569.
Toggweiler, J., Russell, J.L., Carson, S., 2006. Midlatitude westerlies, atmospheric CO2, and climate change during the ice ages. Paleoceanography 21 (2).
Turner, K.J., Fogwill, C.J., McCulloch, R.D., Sugden, D., 2005. Deglaciation of the eastern flank of North Patagonian Icefield and associated continental-scale lake diversion. Geogr. Ann. Phys. Geogr. 87, 363–374.
Turney, C., Roberts, R., De Jonge, N., Prior, C., Wilmshurst, J., McGlone, M., Cooper, J., 2007. Redating the advance of the New Zealand franz josef glacier during the last termination: evidence for asynchronous climate change. Quat. Sci. Rev. 26 (25–28), 3037–3042.
Villa-Martínez, R., Moreno, P.I., Valenzuela, M.A., 2012. Deglacial and postglacial vegetation changes on the eastern slopes of the central Patagonian Andes (47°S). Quat. Sci. Rev. 32, 86–99.
Weaver, A.J., Saenko, O.A., Clark, P.U., Mitrovica, J.X., 2003. Meltwater pulse 1A from Antarctica as a trigger of the Bølling-Allerød warm interval. Science 299 (5613), 1709–1713.